EBioMedicine 29 (2018) 38–46

Contents lists available at ScienceDirect

EBioMedicine

journal homepage: www.ebiomedicine.com

Research Paper

Pathophysiological Characteristics Associated With Epileptogenesis in Human Hippocampal Sclerosis

Hiroki Kitaura [a,*], Hiroshi Shirozu [b], Hiroshi Masuda [b], Masafumi Fukuda [b], Yukihiko Fujii [c], Akiyoshi Kakita [a]

[a] Department of Pathology, Brain Research Institute, Niigata University, 1 Asahimachi, Chuo-ku, Niigata 951-8585, Japan
[b] Department of Neurosurgery, Nishi-Niigata Chuo National Hospital, 1 Masago, Nishi-ku, Niigata 950-2085, Japan
[c] Department of Neurosurgery, Brain Research Institute, Niigata University, 1 Asahimachi, Chuo-ku, Niigata 951-8585, Japan

ARTICLE INFO

Article history:
Received 11 December 2017
Received in revised form 7 February 2018
Accepted 15 February 2018
Available online 21 February 2018

Keywords:
Epilepsy
Hippocampal sclerosis
Subiculum
Kir4.1
Mossy fiber sprouting

ABSTRACT

Mesial temporal lobe epilepsy (MTLE) is the most frequent focal epileptic syndrome in adults, and the majority of seizures originate primarily from the hippocampus. The resected hippocampal tissue often shows severe neuronal loss, a condition referred to as hippocampal sclerosis (HS). In order to understand hippocampal epileptogenesis in MTLE, it seems important to clarify any discrepancies between the clinical and pathological features of affected patients. Here we investigated epileptiform activities *ex vivo* using living hippocampal tissue taken from patients with MTLE. Flavoprotein fluorescence imaging and local field potential recordings revealed that epileptiform activities developed from the subiculum. Moreover, physiological and morphological experiments revealed possible impairment of K^+ clearance in the subiculum affected by HS. Stimulation of mossy fibers induced recurrent trans-synaptic activity in the granule cell layer of the dentate gyrus, suggesting that mossy fiber sprouting in HS also contributes to the epileptogenic mechanism. These results indicate that pathophysiological alterations involving the subiculum and dentate gyrus could be responsible for epileptogenesis in patients with MTLE.

1. Introduction

Because the origin of seizure onset can now be localized accurately (Ryvlin and Rheims, 2016), surgery has become a standard form of treatment for patients with drug-resistant mesial temporal lobe epilepsy (MTLE) (Jobst and Cascino, 2015). In the resected tissue, several degrees of neuronal loss and gliosis (hippocampal sclerosis: HS) is the most commonly encountered pathologic feature (Blümcke and Spreafico, 2012; Cendes et al., 2014). Therefore, there seems little room for doubt that HS is responsible for epileptogenesis in patients with MTLE. However, it is still a matter of debate how such a drastically neuron-depleted region can generate seizure activity. To resolve this question, two major hypotheses have been proposed. First, the role of mossy fiber sprouting (MFS) of dentate granule cells, a characteristic phenomenon whereby neuronal axons sprout and project to themselves, has been suggested (Buckmaster, 2012; Sierra et al., 2015). Although this hypothesis would be convincing from the viewpoint of excitatory recurrent circuit formation, some controversy exists because it is often absent in samples of hippocampal tissue even from patients with severe epilepsy (Longo and Mello, 1998; Pitkänen et al., 2000). The second possibility is spontaneous seizure activity from the subiculum, as suggested from studies of human tissues (Cohen et al., 2002; Chung et al., 2015). Considering that the surgical prognosis of patients with MTLE roughly correlates with the degree of histopathological HS (Bonilha et al., 2012; Mathon et al., 2017), it is important to verify these hypotheses by comparison of cases showing varying degrees of pathological change. One powerful approach for this purpose might be to investigate *ex vivo* the properties of human epileptogenic tissue removed therapeutically by surgery. We have previously reported the usefulness of this methodology for examining human cerebral cortical slices (Kitaura et al., 2011), and in the present investigation described here we also employed human hippocampal slices with sufficiently verified spatial and temporal resolution (Supplementary Fig. 1) to demonstrate the pathomechanisms of epileptogenesis underlying HS.

2. Materials and Methods

All patients provided written informed consent, and the study was performed with the approval of the ethics committees of the Nishi-Niigata Chuo National Hospital and Niigata University. We conducted

Abbreviation: MTLE, mesial temporal epilepsy; HS, hippocampal sclerosis; HFO, high frequency oscillations; Kir4.1, inwardly rectifying potassium channel 4.1; GCL, granule cell layer; CNQX, 6-cyano-7-nitroquinoxaline-2,3-dione; MF, mossy fiber; MFS, mossy fiber sprouting.

* Corresponding author.
E-mail address: kitaura@bri.niigata-u.ac.jp (H. Kitaura).

https://doi.org/10.1016/j.ebiom.2018.02.013

our experiments only with the permission of clinicians and clinical pathologists, and therapeutic judgment was always given priority.

2.1. Clinical Features

Hippocampal specimens were obtained from 31 patients with intractable epilepsy undergoing surgical resection at Nishi-Niigata Chuo National Hospital and Niigata University. For comparison, we used hippocampal tissue taken from five patients in whom the primary seizure onset was detected not in the hippocampus but in the extrahippocampal formations along with some structural lesions (Nagel and Risinger, 1997) (Table 1) (Extrahippocampal onset group; Ex-hipp). Pathological examination showed that these tissues had hardly any detectable neuronal loss, marked gliosis or architectural abnormalities. In the present study, we regarded the Ex-hipp group as the control. Other patients showed varying degrees of hippocampal atrophy in the MRI and exhibited seizure onset from the mesial temporal cortex (MTLE group). We further divided them into two subgroups on the basis of pathological examination: no detectable neuronal loss (hippocampal onset without HS group; No-HS) and obvious neuronal devastation (corresponding to the classical form, and defined as HS) (Supplementary Fig. 2). Although obvious atrophy of the hippocampus was demonstrated by MRI in HS (100%), none was detected in No-HS (Table 1). The age at surgery in the HS group was significantly higher than in the Ex-hipp group, and seizure duration tended to be longer in the HS group than in the Ex-hipp group, although not to a significant degree ($p = 0.058$, ANOVA) (Supplementary Fig. 3).

2.2. Slice Preparations and Maintenance

All of the MTLE patients underwent anteromedial temporal lobectomy with en bloc resection of the hippocampus. About 3–4 cm of hippocampal tissue was resected longitudinally, and coronal brain blocks about 5 mm thick were sectioned at 1 cm from the head of the hippocampus in the operating room. We prepared brain slices for physiological experiments as described previously (Supplementary Fig. 4) (Kitaura et al., 2011).

2.3. Flavoprotein Fluorescence Imaging Ex Vivo

Each slice was transferred to a recording chamber and perfused continuously with oxygenated ACSF at a flow rate of 2 ml min^{-1}. A stimulating electrode (Teflon-coated platinum wire 76 μm in diameter, #772000, A-M Systems, WA, USA) was placed in the granule cell layer of the dentate gyrus (DG), center of the CA4, the pyramidal cell layer of the CA1, 2 and 3 subfields, or the subiculum. Then biphasic current pulses were applied (±350 μA; duration of each phase: 200 μs) at 20 Hz for 1 s. Endogenous green fluorescence images ($\lambda = 510–550$ nm) in blue light (470–490 nm) were recorded as flavoprotein fluorescence signals with a cooled CCD camera system (AQUACOSMOS, Ratio with ORCA-AG Camera, Hamamatsu Photonics, Japan). These images (336×256 pixels 16-bit depth) were recorded at 100-ms intervals for 10 s. Images were obtained in 8 trials repeated at 1-min intervals, and the results were averaged. Each pixel in the averaged images was normalized by a corresponding pixel that represented the mean of 10 images obtained immediately before stimulus onset. Increases in the

Table 1
Patient data.

Control								
Case no.	Age at surgery (yr)	Duration of seizures (yr)	MRI findings in hippocampus	Pathological diagnosis	Neuronal loss			Watson grade
					CA4	CA1	DG	
E-1	15	10	–	TS (T)	–	–	–	0
E-2	2	1	–	FCD type II (T)	–	–	–	0
E-3	21	2	–	Ependymoma (T)	–	–	–	0
E-4	20	7	–	Ganglioglioma (T)	–	–	–	0
E-5	26	3	–	No significant alterations	–	–	–	0
No-HS								
N-1	51	13	–	No HS	–	–	–	0
N-2	12	6	–	No HS	–	–	–	1
N-3	25	16	–	No HS	–	–	–	1
N-4	33	12	–	No HS, Polymicrogyria (T)	–	–	–, dis	0
N-5	19	2	–	No HS	–	–	–	1
N-6	46	19	–	No HS	–	–	–	1
HS								
S-1	32	19	Atrophy	HS	+++	+++	+, dis	4
S-2	17	8	Atrophy	HS, FCD type I (T)	+++	+++	+, dis	4
S-3	27	3	Atrophy	HS	+++	+++	+, dis	4
S-4	37	22	Atrophy	HS	+++	+++	++, dis	4
S-5	32	5	Atrophy	HS, FCD type I (T)	+++	+++	–, dis	4
S-6	53	43	Atrophy	HS	+++	+++	++, dis	4
S-7	64	44	Atrophy	HS	+++	+++	–, dis	4
S-8	42	2	Atrophy	HS, FCD type I (T)	+++	+++	+, dis	4
S-9	39	23	Atrophy	HS, FCD type I (T)	+++	+++	+, dis	4
S-10	36	33	Atrophy	HS, FCD type I (T)	+++	+++	+, dis	4
S-11	23	6	Atrophy	HS, FCD type I (T)	+++	+++	+, dis	4
S-12	36	7	Atrophy	HS, FCD type I (T)	+++	+++	–, dis	4
S-13	14	4	Atrophy	HS	++	+++	–, dis	3
S-14	27	16	Atrophy	HS, FCD type I (T)	+++	+++	+, dis	4
S-15	43	34	Atrophy	HS	+++	+++	+, dis	4
S-16	10	6	Atrophy	HS, FCD type I (T)	+++	+++	+, dis	4
S-17	32	15	Atrophy	HS, FCD type I (T)	++	+++	+, dis	3
S-18	30	28	Atrophy	HS	+++	+++	–, dis	4
S-19	52	17	Atrophy	HS	+++	+++	+, dis	4
S-20	44	36	Atrophy	HS, FCD type I (T)	++	+++	–, dis	3

HS: Hippocampal sclerosis, EFS: End folium sclerosis, (T): Temporal cortex, TS: Tuberous Sclerosis, FCD: Focal cortical dysplasia, dis: granule cell dispersion. +: mild, ++: moderate, +++: severe neuronal loss.

fluorescence were shown using a pseudo-color scale. For quantitative analysis of fluorescence changes, a circular ROI (region of interest, diameter 0.5 mm) was placed at the peak of the responding area, and the maximal amplitude during the time course of the response was used as the peak amplitude.

2.4. Field Potential Recordings

Field potential recordings were performed using a slice different from that used for the flavoprotein fluorescence imaging experiment. Multiple simultaneous extracellular recordings were performed with Teflon-coated tungsten electrodes (1.0 MΩ; USK-20, Unique Medical, Japan) positioned in the CA1, subiculum and granular cell layer of the dentate gyrus. Signals were amplified 10,000 times and passed through a 1.5–10-kHz band-pass filter with an amplifier (MEG-2100, Nihon Kohden, Tokyo, Japan). Mains hum was removed with a 50-Hz notch filter. Spontaneous field potentials were recorded during 10 min at a sampling rate of 10 kHz. The signal was input to a computer *via* an analog-digital converter (PowerLab, AD Instruments, Australia) for later analyses.

Fast Fourier Transform (FFT) was performed on 1024 data points (102 ms; frequency resolution 9.8 Hz) at each time step with LabChart 7 (AD Instruments, Australia). Ten consecutive FFT data for the events were aligned at the initial peak of the event temporally and averaged using a script written in-house for MATLAB (MathWorks, USA).

2.5. Histological Procedures

We used a brain block corresponding to the mirror surface of each slice that had been used in the physiological examination. The blocks were fixed with phosphate-buffered 20% formalin and embedded in paraffin wax. Sections 4 μm thick were cut and stained by the Klüver-Barrera method or immunostained with the following primary antibodies: rabbit polyclonal antibody against glial fibrillary acidic protein (GFAP) (Z0334, Dako; 1:1000), Kir 4.1 (APC-035, Alomone labs; 1:4000; autoclaving at 120 °C in 0.05 M citrate buffer for 10 min). The signals were detected using immunofluorescent secondary antibodies (Alexa Fluor 568 goat anti-rabbit and Alexa Fluor 488 goat anti-mouse) using confocal microscopy (FV3000RS, Olympus, Tokyo). The detailed protocols of Timm staining and quantitative analysis are described in the Supplementary Methods.

2.6. Data Analysis

All data are presented as the mean ± SEM, except in Supplementary Fig. 3. Comparisons between two groups were analyzed using unpaired Student's *t*-test, while multi-group comparisons were analyzed using one-way ANOVA followed by Tukey-Kramer *post hoc* test. Differences at $p < .05$ were considered significant.

3. Results

3.1. Enhanced Neuronal Activities in the Subiculum in MTLE Group

To investigate the propagation of ictal-like activities, we stimulated hippocampal slice preparations electrically (20 Hz, 1 s) in each hippocampal subfield, and found that evoked responses appeared consistent with the histological features of neuronal presentation and depression (Fig. 1a, Supplementary Fig. 2). Interestingly, although these responses appeared to be almost similar in each subfield in the Ex-hipp group, we noticed that in the HS and No-HS groups the peak amplitude and fluorescence response areas in the subiculum were significantly greater than those in the Ex-hipp group (Fig. 1b, c).

Next, we recorded long-term local field potentials (LFPs) from the subiculum, which are known to be possibly associated with interictal-like activity *in vivo* (Cohen et al., 2002). In the No-HS and HS groups, we found spontaneous rhythmic activities similar to those documented previously (Huberfeld et al., 2011). In addition, we noticed that these activities were present in the CA1 of some (2 out of 4) cases in the No-HS group (Fig. 2a). No spontaneous activity was observed in any of the other subfields. In the No-HS group, the activities in the subiculum and CA1 were temporarily co-related, the activity in the subiculum always being followed by that in CA1 (Fig. 2b), suggesting that activity generated primarily in the subiculum was able to propagate into CA1 *via* feedback projection from the subiculum to CA1 (Harris and Stewart, 2001). The number of events in the subiculum recorded during 10 min in both the No-HS and HS groups was significantly higher than in the Ex-hipp group, and moreover, the number in the HS group was significantly higher than that in the No-HS group (Fig. 2c). When a high-pass filter (100 Hz) was applied to these single events, we clearly recognize obvious high-frequency components in No-HS and HS group (Fig. 2d). Time-frequency power-spectral analysis demonstrated high-frequency oscillations (HFO) as a clear spectral spots ranging around 100 Hz in these groups (Fig. 2e).

3.2. Impairment of K^+ Clearance in the Subiculum of HS

As the extracellular K^+ concentration ($[K^+]_o$) can increase up to 10–12 mM during ictal state activities (Heinemann and Lux, 1977; Rimmele et al., 2017), we changed $[K^+]_o$ from 3 to 12 mM during LFP recordings in the subiculum in the No-HS and HS groups to compare the property of HFO. The number of events gradually increased in accordance with $[K^+]_o$, although the amplitude of the events did not clearly change (Fig. 3a). In the HS group, the frequency at peak power of HFO during each event showed a marked increase in accordance with $[K^+]_o$, reaching the fast ripple band (>250 Hz) at 12 mM $[K^+]_o$, and was significantly higher than in the No-HS group (Fig. 3b, c). Sensitivity to $[K^+]_o$ in the HS group suggested impairment of the mechanism for clearance of excessive extracellular K^+, *i.e.* spatial K^+ buffering (Kofuji and Newman, 2004). Kir 4.1, expressed in astrocytes, is a molecule playing a pivotal role in this mechanism (Heuser et al., 2012; Steinhauser et al., 2016). Consistent with this, only in the HS group, immunoreactivity for Kir4.1 in astrocytes in the subiculum labeled for GFAP, an astrocytic marker, was significantly weak (Fig. 3d, e), even though immunoreactivity for both proteins was similarly maintained in the No-HS and Ex-hipp groups, and in the granule cell layer (GCL) in all of the HS, No-HS, and Ex-hipp groups (Supplementary Fig. 5).

3.3. MFS Requires Both Intrinsic Seizure Activity and Neuronal Loss

In the No-HS group, electrical stimulation of the CA4 subfield induced a local fluorescence response at the stimulation point, and this gradually spread to reach the GCL (Fig. 4a, *MF Stim*). Distinct from this, in the HS group, the primary response was observed in the GCL, rather than at the stimulation point in the CA4 subfield (Fig. 4a, B; Fig. 1a, *arrow*), suggesting the occurrence of MFS. Consistent with this physiological feature, morphological analysis with Timm stain revealed a diffuse signal representing the synaptic buttons of mossy fibers in the inner molecular layer of the dentate gyrus only in the HS group (Fig. 4a, *Timm stain*). These retroactive fluorescence responses of the GCL in HS were significantly suppressed by application of CNQX, a non-NMDA glutamate receptor antagonist (Fig. 4c), indicating that they are recurrent fluorescence responses containing trans-synaptic components. In the HS group, LFPs in the GCL evoked by MF stimulation were also consistent with the fluorescence responses, where the first deflection (antidromic component) was followed by repetitive deflections (orthodromic component), and the later deflections were almost totally abolished by CNQX application (Fig. 4d). Furthermore, the amplitude of the recurrent activities was clearly correlated with the width of the GCL (Fig. 4e), consistent with a previous morphological study (Schmeiser et al., 2017). Aberrant thickness of the GCL is a feature

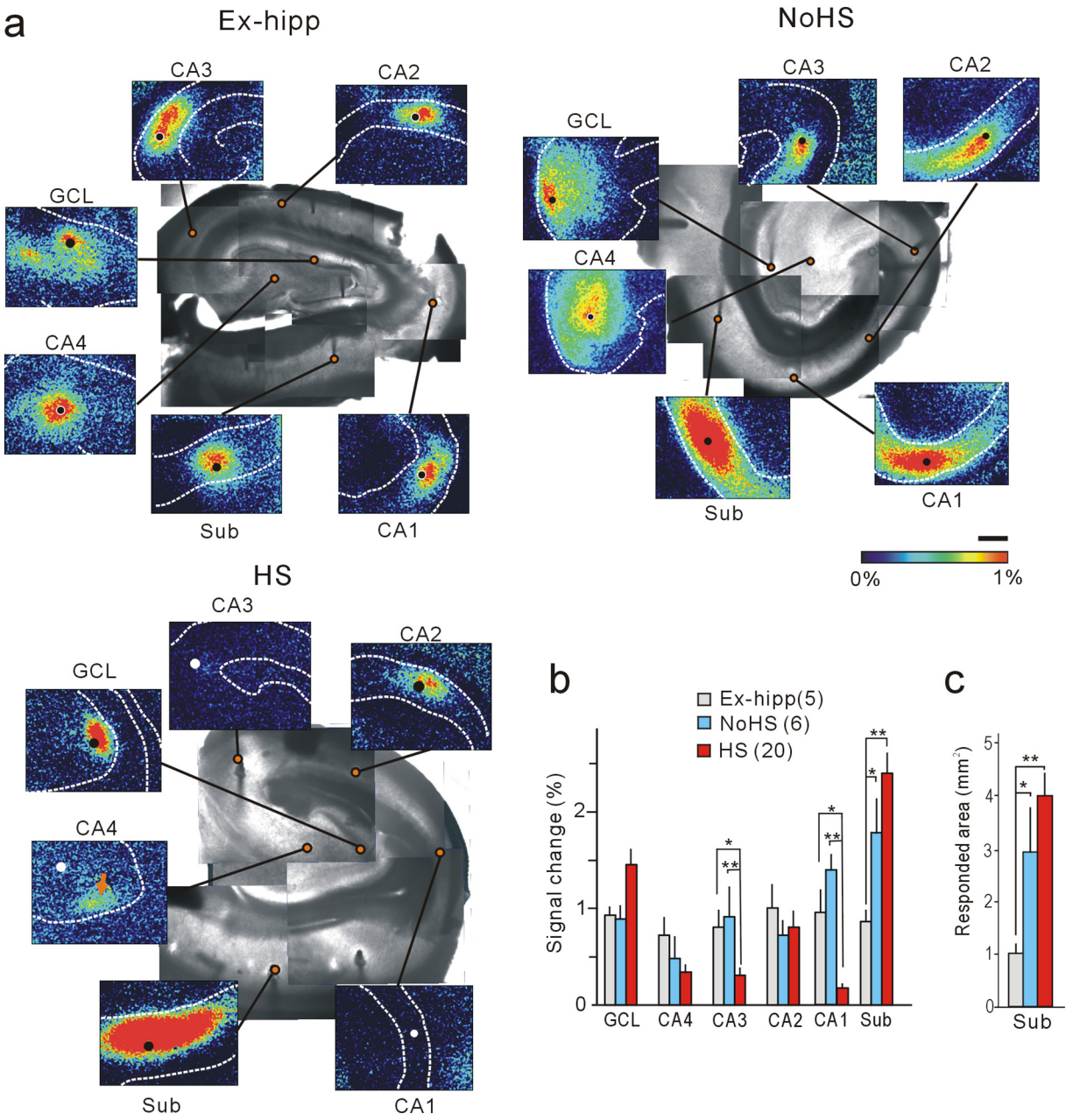

Fig. 1. Evoked responses indicating enhanced activity in the subiculum, revealed by flavoprotein fluorescence imaging. (a) Representative images of tissue from each of the Ex-hipp, No-HS and HS groups. Solid circles indicate stimulation points. Note the enhanced responses in the subiculum of patients with No-HS and HS. In HS, stimulation of mossy fibers elicits a response in the dentate granule cell layer (*arrow* in the panel "CA4"). All images were obtained at 1.2 s after stimulation onset. Scale bar: 1 mm. (b, c) Quantitative analysis of the peak amplitudes (b) and responded area >0.5% of the subiculum (c) are shown. Error bars, S.E.M. *$p < .05$ and **$p < .01$, Tukey-Kramer test after one-factor ANOVA.

associated with MTLE, characterized by granular cell dispersion (Blümcke et al., 2013; Thom, 2014).

4. Discussion

In the present study, patients in the HS group were significantly older at surgery and tended to have a longer seizure duration than those in the Ex-hipp group (Supplementary Fig. 3). One of the reasons why the latter did not reach a significant value ($p = .058$) may have been the large mismatch in the number of patients in the two groups. Our data are consistent with a previous report suggesting that patients with earlier seizure onset and a longer duration of epilepsy have more severe HS (Fuerst et al., 2001). Although the Ex-hipp group could not be regarded as "normal" controls, they were considered to be "disease controls" and also had drug-resistant epilepsy. This made them more suitable for comparison, as our focus was on a unique form of intra-hippocampal epileptogenicity.

We evaluated neuronal activities in hippocampal tissue *ex vivo* using flavoprotein fluorescence imaging, which examines activity-dependent changes in flavoprotein fluorescence (Kitaura and Kakita, 2013). Flavoproteins are abundantly present in the mitochondria of neurons, and changes in their fluorescence have been used as an indicator of local metabolic changes in brain tissue (Theyel et al., 2010; Tohmi et al., 2009). Because this technique requires no exogenous dyes, it has a simple experimental procedure and avoids the disadvantages of dye-related techniques. Therefore, it offers advantages such as high stability and reproducibility for long experimental periods, making it suitable for *ex vivo* investigations of human brain tissue. The subfields that

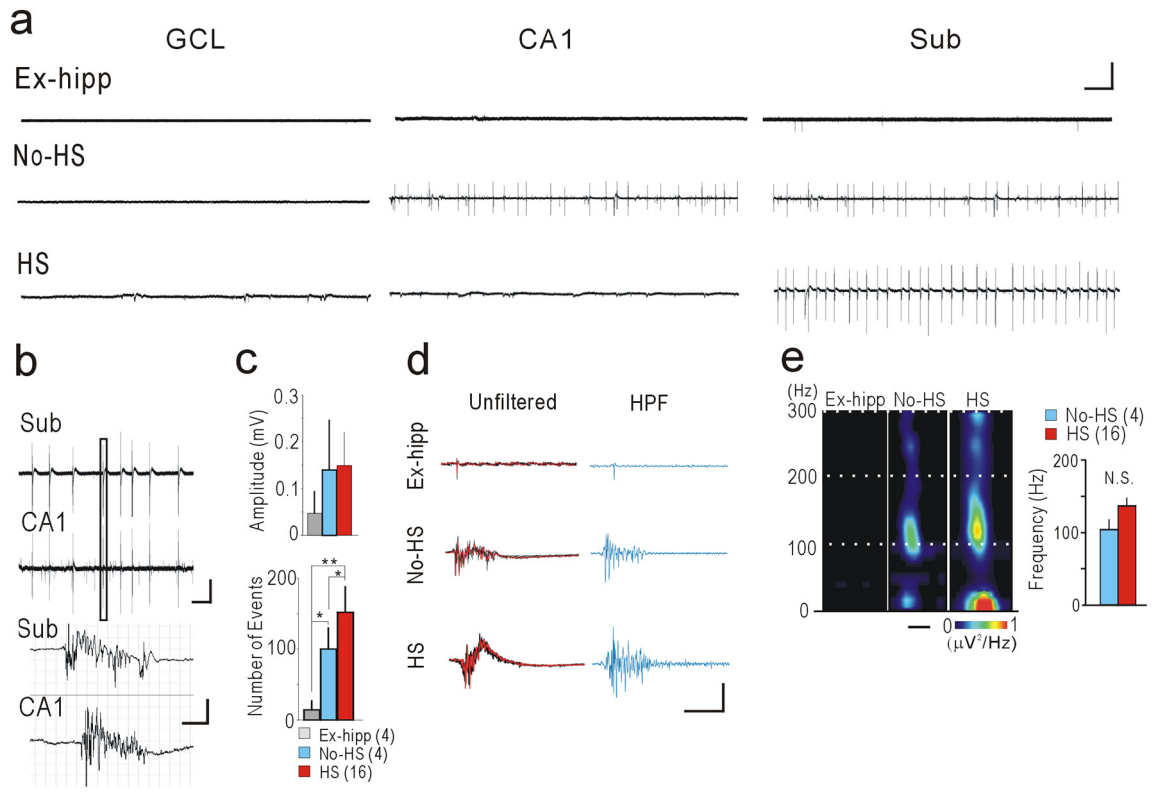

Fig. 2. Spontaneous field potential recordings reveal epileptiform activities and HFOs components in the subiculum. (a) Representative traces of long-term LFP showing spontaneous activities in each subfields. Calibration: 0.1 mV, 10 s. (b) Coupling activities between the subiculum and CA1 in No-HS. Magnified traces of a single event (indicated by *box* in *upper panel*) are shown in the *lower panel*. Calibration: 0.1 mV, 10 s (*upper panel*), 50 ms (*lower panel*). (c) Amplitude (*upper panel*) and number of events (*lower panel*) of LFP analyzed quantitatively in the subiculum during 10-min recordings. Number of events in No-HS and HS is significantly higher than in the Ex-hipp, even though the amplitudes are not significantly different. *$p < .05$ and **$p < .01$, Tukey-Kramer test after one-factor ANOVA. N.S.: not significant. (d) Magnified traces of single LFP events in the subiculum. Five consecutive traces are overlapped (the last trace is indicated by the *red line*), indicating similar waveforms (*unfiltered*). Traces with application of a high-pass filter (*HPF*) at 100 Hz. Calibration: 0.1 mV (*unfiltered*), 50 μV (*HPF*), 50 ms. (e) Representative time-frequency spectral analysis of 10 averaged consecutive events in the subiculum demonstrates clear spot-like activity (*upper panel*). Scale bar: 100 ms. The frequency at peak power does not differ significantly (*lower panel*). Error bars, S.E.M.

demonstrated flavoprotein fluorescence were closely correlated with the distribution of neuronal preservation, suggesting that the signal changes require neuronal activity.

As a result, we detected not only evoked (Fig. 1) but also spontaneous enhanced activities in the subiculum (Fig. 2), which were possibly associated with the interictal spikes appearing on ECoG of patients with MTLE, as demonstrated previously (Cohen et al., 2002). Furthermore, we detected discrete HFO, a biomarker suggesting the delineated boundaries of epileptogenic regions *in vivo* (Bragin et al., 2010; Jacobs et al., 2009), in hippocampal slices from patients with not only in HS but also in No-HS (Fig. 2d, e). These results suggested that the epileptogenic mechanism had already developed in the subiculum in the No-HS group, where coupling spontaneous activities were also observed in CA1, suggesting that reciprocal activation between CA1 and the subiculum would be important for epileptogenesis (Fig. 5). On the other hand, in HS, severe neuronal loss in CA1 would interrupt the trisynaptic pathway and the inhibited input into the subiculum might contribute to the enhancement of internal excitability. As the subiculum is a key structure involved in hippocampal output to extensive brain regions (Ishizuka, 2001), excessive excitability in the subiculum could lead to intractable epilepsy.

We also found fast ripples, very high frequency oscillations of >250 Hz (Ogren et al., 2009), in the presence of 12 mM $[K^+]_o$ in slices from the HS groups, but not in slices from the No-HS group (Fig. 3b, c). This finding seems consistent with the results of an *in vivo* clinical ECoG study (Staba et al., 2007) in which there was a significant inverse correlation between the occurrence rate of fast ripples, but not ripples, and hippocampal volume, as analyzed by MRI. As our results were derived from resected hippocampal tissue alone, clinically observed fast ripples may be generated inside the hippocampus, or at least partially so. The vulnerability to $[K^+]_o$ increment observed in the HS group was consistent with the morphological profile of marked reduction of Kir 4.1-immunoreactivity in astrocytes in the subiculum (Fig. 3d, e). An increase of $[K^+]_o$ would influence neuronal excitability, and then high-frequency neuronal activity would in turn lead to further transient accumulation of $[K^+]_o$. Therefore, if $[K^+]_o$ cannot be immediately compensated through Kir 4.1, a vicious cycle may ensue, readily leading to status epilepticus. In the HS group, reduction of the potassium buffering

Fig. 3. Different responses to potassium concentrations in the subiculum of the HS and No-HS groups. (a) Number (*left*) and amplitude (*right*) of events during 10-min LFP recordings in the presence of 6, 9, and 12 mM $[K^+]_o$ are normalized to those recorded in the presence of 3 mM $[K^+]_o$. (b) Representative images of time-frequency power-spectral analysis of 10 averaged consecutive events with changes in $[K^+]_o$. Note the ascending spots in HS. Scale bar: 100 ms. (c) Quantification of changing the frequencies at peak power in the presence of 3, 6, 9, and 12 mM $[K^+]_o$. (a–c) In these studies, we used two slices per patient. (*n*) indicates the number of slices. *$p < .05$, Tukey-Kramer test after one-factor ANOVA. (d) Double immunofluorescence images of the subiculum indicating loss of Kir 4.1 immunoreactivity (*red*) in the processes of GFAP (*green*)-positive cells in HS. Scale bar: 50 μm. (e) Quantitative analysis of the total area of immunofluorescence. The immunofluorescence area of Kir4.1 was normalized to that of GFAP. *$p < 0.05$, Tukey-Kramer test after one-factor ANOVA. Lower panels are sample images of the original image (upper) and the extracted area for calculation (Red area: lower). Scale bars: 25 μm. Error bars, S.E.M.

reserve might exacerbate the irritability of the neural circuits, inducing severe epileptic discharges such as fast ripples. In the present study, we were unable to address other possible influences on the dynamics of $[K^+]_o$ such as defects in Na^+/K^+ ATPase (Grisar et al., 1992), voltage-dependent K^+ channels (Biervert et al., 1998) or the BK channel (Du et al., 2005). On the other hand, we cannot exclude possible

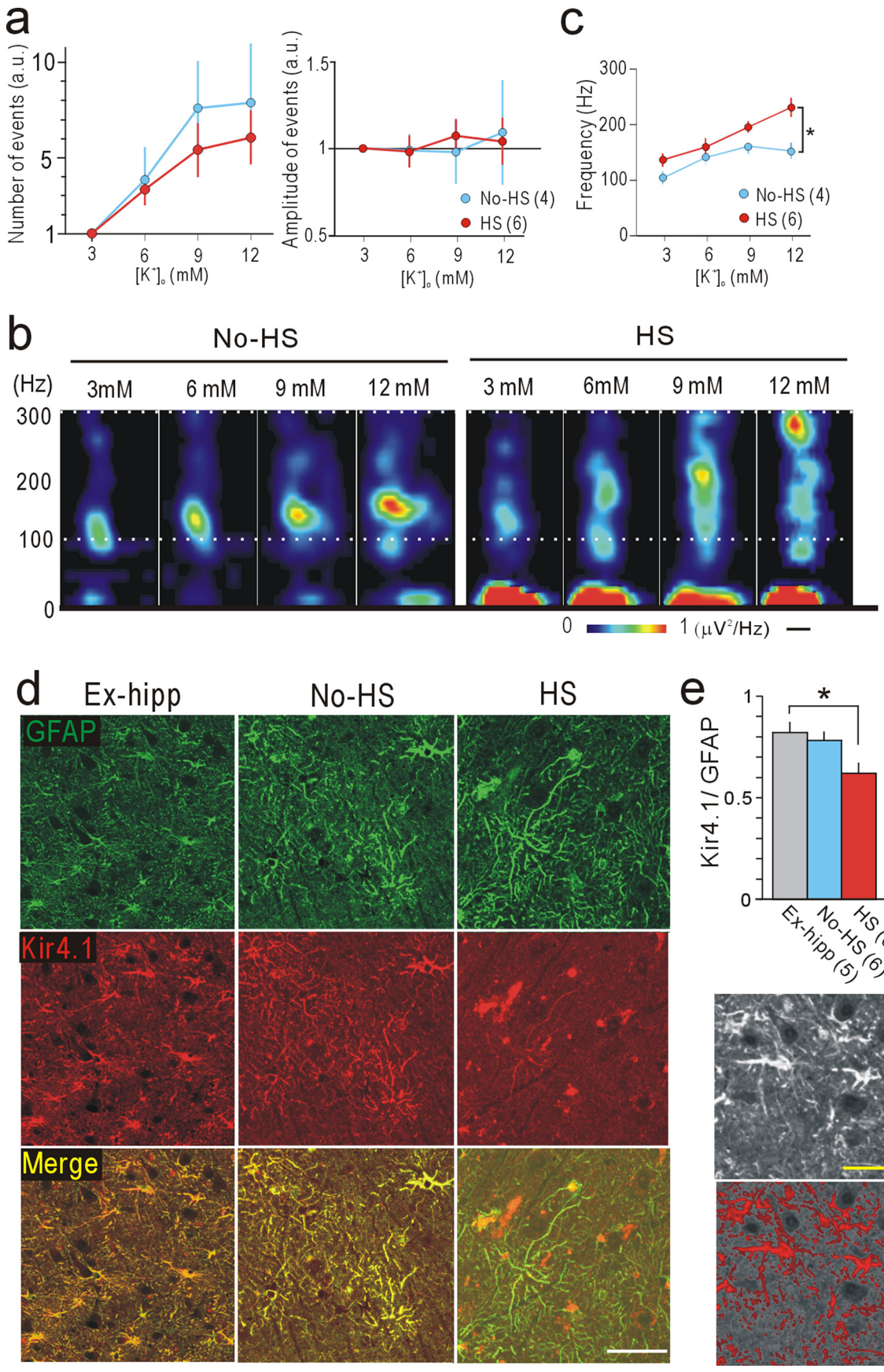

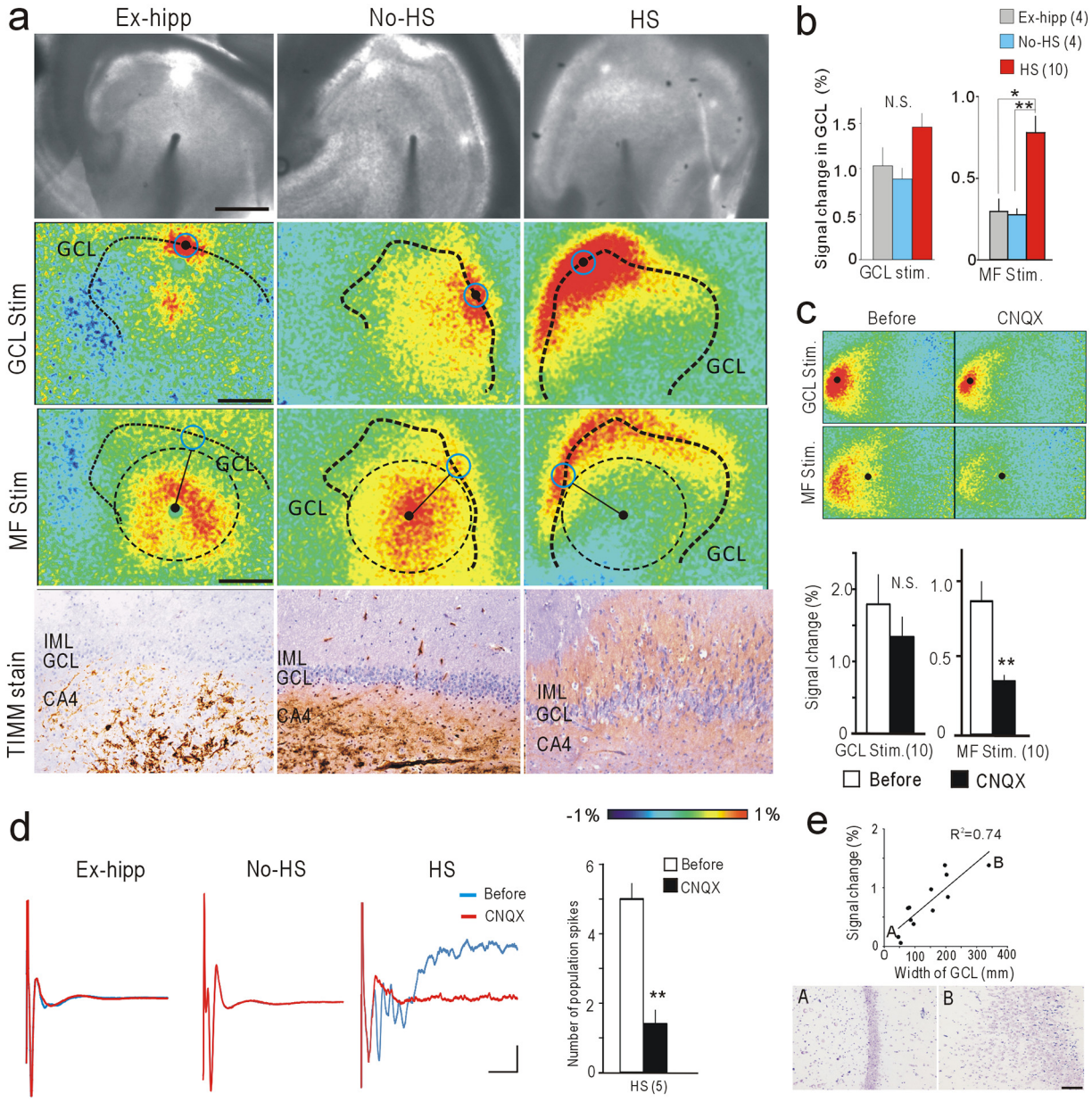

Fig. 4. Recurrent excitatory activities in the GCL of HS. (a) Flavoprotein fluorescence imaging and Timm staining in the DG. Scale bars: 1 mm (flavoprotein fluorescence imaging) and 100 μm (Timm staining). ROIs on the GCL (blue circle) were placed equidistant from the stimulation point (black filled circle). (b) Quantitative analysis of ROIs in (a). Retroactive GCL responses upon MF stimulation were significantly larger in HS (*right*), but not upon direct GCL stimulation (*left*). (c) Effect of CNQX on retroactive activities in GCL evoked by MF stimulation in HS. Flavoprotein fluorescence responses were significantly suppressed by MF stimulation, but not by direct GCL stimulation. (d) LFP at GCL upon MF stimulation before and after CNQX application. Repetitive deflections were observed only in HS, and were clearly abolished by CNQX. The numbers of spikes were compared before and after CNQX application in HS (n = 5). (e) Correlation between signal changes in GCL and width of GCL in HS. Points A and B indicated in the graph correspond to the images in the lower panels. Scale bar: 100 μm. Error bars, S.E.M. $^{*}p < 0.05$, $^{**}p < 0.01$; by One-way ANOVA with Tukey-Kramer test (b) or paired *t*-test (c, d). N.S.: not significant.

mechanisms of enhancement in the subiculum other than impairment of potassium buffering, such as selective loss of parvalbumin neurons (Andrioli et al., 2007) or alteration of the neuronal response to GABA in the subiculum (Huberfeld et al., 2011; Cohen et al., 2002). All of these mechanisms involve neuronal malfunction, whereas the impairment of potassium buffering suggested here involves the function of glia. However, these mechanisms may not be mutually contradictory, and each may contribute in some way to epileptogenic activity.

In the GCL of the HS group, we found recurrent trans-synaptic activity (Fig. 4), presumably as a consequence of MFS. For induction of MFS, both intrinsic seizure activity and neuronal loss in the CA3-4 subfield would be required (Proper et al., 2000; Thom, 2014). In line with these previous reports, MFS was not found in the No-HS group in the present study (Fig. 4a–d). Moreover, the changes in signal in the GCL were well correlated with the degree of dispersion (Fig. 4e). Interpretation of the role of MFS is somewhat controversial. MFS is considered to elicit hyperexcitability of GCL cells through the establishment of positive feedback circuits (Buckmaster, 2012), although another study has referred to an opposite effect whereby it also projects to inhibitory neurons to establish negative feedback circuits (Kotti et al., 1997). As we found that hyperexcitability of GCL neurons appeared to be dependent on the degree of MFS, it is possible that MFS may contribute to the epileptogenesis in HS. Considering the possible contribution of the MFS, creating an abnormal circuit that amplifies neuronal activity, surgical resection of the atrophic hippocampus with MFS would be needed for patients with HS. On the other hand, for patients with No-HS, a

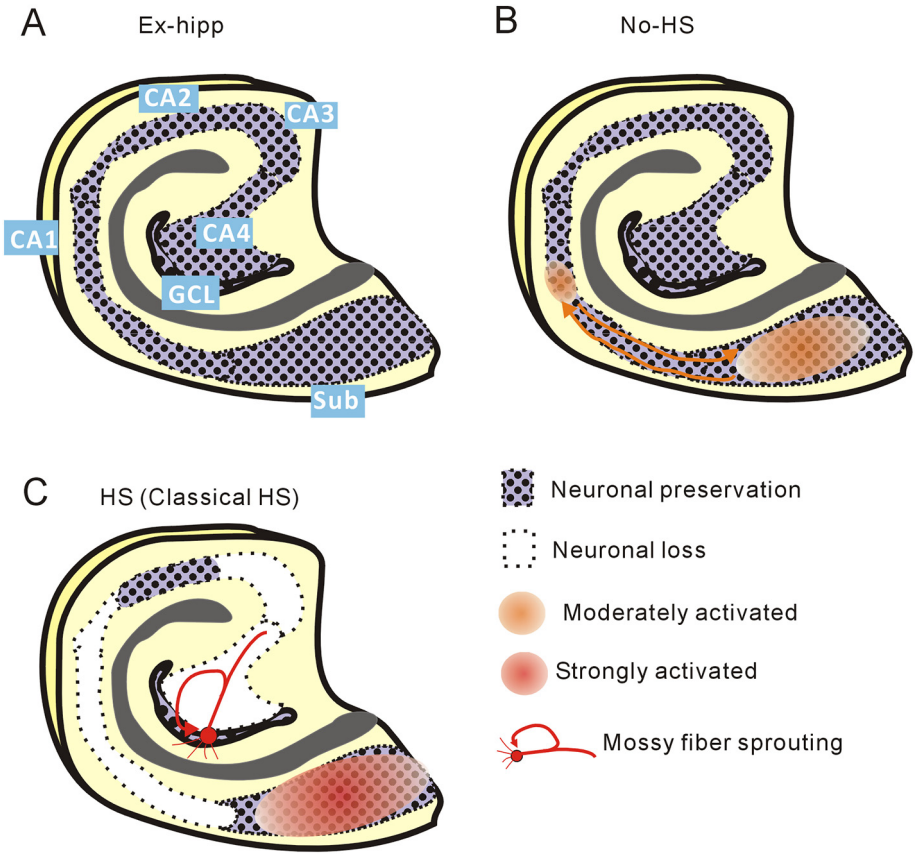

Fig. 5. Schematic representation of the results. (a) Control hippocampus showing anatomical orientation. (b) No-HS. Enhanced activities are initiated in the subiculum and extend retroactively to the CA1. (c) HS. Epileptogenesis in the subiculum and MFS in GCL are evident.

minimally invasive surgical approach involving transection of the circuit between the subiculum and the CA1 might be effective. Detailed presurgical MRI examination of the hippocampal volume (Table 1) may be informative for determining which approach would be necessary for individual patients with MTLE.

In conclusion, examination of hippocampal specimens from humans with epilepsy offers considerable advantages for investigating the correlation between pathology and functional abnormality, although it has a limitation in that it cannot be used to consider issues beyond the scope of the tissue being studied. Our findings suggest that the pathophysiological mechanisms responsible for epilepsy may differ depending on the degree of HS (Fig. 5).

Acknowledgement

The authors thank Prof. James E. Goldman, Department of Pathology, Columbia University, for useful comments on the manuscript.

Funding Sources

This work is supported by JSPS Grants-in aid for Scientific Research (C: 25870252; H. Kitaura and A: 25250008; A. Kakita) and the Japan Agency for Medical Research and Development (AMED; 17ek0109120h0003).

Conflicts of Interest

The authors have no competing financial interests to declare.

Author Contributions

H·K. performed imaging and electrophysiological experiments. H.S., H.M., M.F. and Y.F. evaluated the clinical information. A.K. performed the pathological evaluations. H.K and A.K. designed the study and wrote the paper.

Appendix A. Supplementary Data

Supplementary data to this article can be found online at https://doi.org/10.1016/j.ebiom.2018.02.013.

References

Andrioli, A., Alonso-Nanclares, L., Arellano, J.I., DeFelipe, J., 2007. Quantitative analysis of parvalbumin-immunoreactive cells in the human epileptic hippocampus. Neuroscience 149, 131–143.
Biervert, C., Schroeder, B.C., Kubisch, C., Berkovic, S.F., Propping, P., Jentsch, T.J., et al., 1998. A potassium channel mutation in neonatal human epilepsy. Science (5349), 403–406.
Blümcke, I., Spreafico, R., 2012. Cause matters: a neuropathological challenge to human epilepsies. Brain Pathol. 22, 347–349.
Blümcke, I., Thom, M., Aronica, E., Armstrong, D.D., Bartolomei, F., Bernasconi, A., et al., 2013. International consensus classification of hippocampal sclerosis in temporal lobe epilepsy: a task force report from the ILAE commission on diagnostic methods. Epilepsia 54, 1315–1329.
Bonilha, L., Martz, G.U., Glazier, S.S., Edwards, J.C., 2012. Subtypes of medial temporal lobe epilepsy: influence on temporal lobectomy outcomes? Epilepsia 53, 1–6.
Bragin, A., Engel Jr., J., Staba, R.J., 2010. High-frequency oscillations in epileptic brain. Curr. Opin. Neurol. 23, 151–156.
Buckmaster, P.S., 2012. Mossy fiber sprouting in the dentate gyrus. In: Noebels, J.L., et al. (Eds.), Jasper's Basic Mechanisms of the Epilepsies, 4th ed. National Center for Biotechnology Information, Bethesda (MD).
Cendes, F., Sakamoto, A.C., Spreafico, R., Bingaman, W., Becker, A.J., 2014. Epilepsies associated with hippocampal sclerosis. Acta Neuropathol. 128, 21–37.
Chung, S., Spruston, N., Koh, S., 2015. Age-dependent changes in intrinsic neuronal excitability in subiculum after status epilepticus. PLoS One 10, e0119411.
Cohen, I., Navarro, V., Clemenceau, S., Baulac, M., Miles, R., 2002. On the origin of interictal activity in human temporal lobe epilepsy in vitro. Science 298, 1418–1421.
Du, W., Bautista, J.F., Yang, H., et al., 2005. Calcium-sensitive potassium channelopathy in human epilepsy and paroxysmal movement disorder. Nat. Genet. 37, 733–738.
Fuerst, D., Shah, J., Kupsky, W.J., Johnson, R., Shah, A., Hayman-Abello, B., et al., 2001. Volumetric MRI, pathological, and neuropsychological progression in hippocampal sclerosis. Neurology 57, 184–188.

Grisar, T., Guillaume, D., Delgado-Escuet, A.V., 1992. Contribution of Na^+,K^+-ATPase to focal epilepsy. Epilepsy Res. 12, 141–149.
Harris, E., Stewart, M., 2001. Propagation of synchronous epileptiform events from subiculum backward into area CA1 of rat brain slices. Brain Res. 895, 41–49.
Heinemann, U., Lux, H.D., 1977. Ceiling of stimulus induced rises in extracellular potassium concentration in the cerebral cortex of cat. Brain Res. 120 (1977), 231–249.
Heuser, K., Eid, T., Lauritzen, F., Thoren, A.E., Vindedal, G.F., Taubøll, E., et al., 2012. Loss of perivascular Kir4.1 potassium channels in the sclerotic hippocampus of patients with mesial temporal lobe epilepsy. J. Neuropathol. Exp. Neurol. 71, 814–825.
Huberfeld, G., Menendez de la Prida, L., Pallud, J., Cohen, I., Le Van Quyen, M., Adam, C., et al., 2011. Glutamatergic pre-ictal discharges emerge at the transition to seizure in human epilepsy. Nat. Neurosci. 14, 627–635.
Ishizuka, N., 2001. Laminar organization of the pyramidal cell layer of the subiculum in the rat. J. Comp. Neurol. 435, 89–110.
Jacobs, J., Levan, P., Châtillon, C.E., Olivier, A., Dubeau, F., Gotman, J.J., 2009. High frequency oscillations in intracranial EEGs mark epileptogenicity rather than lesion type. Brain 132, 1022–1037.
Jobst, B.C., Cascino, G.D., 2015. Resective epilepsy surgery for drug-resistant focal epilepsy: a review. JAMA 313, 285–293.
Kitaura, H., Kakita, A., 2013. Optical imaging of human epileptogenic tissue in vitro. Neuropathology 33, 469–474.
Kitaura, H., Hiraishi, T., Murakami, H., Masuda, H., Fukuda, M., Oishi, M., et al., 2011. Spatiotemporal dynamics of epileptiform propagations: imaging of human brain slices. NeuroImage 58, 50–59.
Kofuji, P., Newman, E.A., 2004. Potassium buffering in the central nervous system. Neuroscience 129, 1045–1056.
Kotti, T., Riekkinen, P.J., Miettinen, R., 1997. Characterization of target cells for aberrant mossy fiber collaterals in the dentate gyrus of epileptic rat. Exp. Neurol. 146, 323–330.
Longo, B.M., Mello, L.E., 1998. Supragranular mossy fiber sprouting is not necessary for spontaneous seizures in the intrahippocampal kainate model of epilepsy in the rat. Epilepsy Res. 32, 172–182.
Mathon, B., Bielle, F., Samson, S., Plaisant, O., Dupont, S., Bertrand, A., et al., 2017. Predictive factors of long-term outcomes of surgery for mesial temporal lobe epilepsy associated with hippocampal sclerosis. Epilepsia 58, 1473–1485.
Nagel, A.G., Risinger, M.W., 1997. Ictal semiology in hippocampal versus extrahippocampal temporal lobe epilepsy. Brain 120, 183–192.
Ogren, J.A., Wilson, C.L., Bragin, A., Lin, J.J., Salamon, N., Dutton, R.A., et al., 2009. Three-dimensional surface maps link local atrophy and fast ripples in human epileptic hippocampus. Ann. Neurol. 66, 783–791.
Pitkänen, A., Nissinen, J., Lukasiuk, K., Jutila, L., Paljärvi, L., Salmenperä, T., et al., 2000. Association between the density of mossy fiber sprouting and seizure frequency in experimental and human temporal lobe epilepsy. Epilepsia 41, S24–29.
Proper, E.A., Oestreicher, A.B., Jansen, G.H., Veelen, C.W., van Rijen, P.C., Gispen, W.H., de Graan, P.N., 2000. Immunohistochemical characterization of mossy fibre sprouting in the hippocampus of patients with pharmaco-resistant temporal lobe epilepsy. Brain 123, 19–30.
Rimmele, T.S., Rocher, A.B., Wellbourne-Wood, J., Chatton, J.Y., 2017. Control of glutamate transport by extracellular potassium: basis for a negative feedback on synaptic transmission. Cereb. Cortex 27, 3272–3283.
Ryvlin, P., Rheims, S., 2016. Predicting epilepsy surgery outcome. Curr. Opin. Neurol. 29, 182–188.
Schmeiser, B., Zentner, J., Prinz, M., Brandt, A., Freiman, T.M., 2017. Extent of mossy fiber sprouting in patients with mesiotemporal lobe epilepsy correlates with neuronal loss and granule cell dispersion. Epilepsy Res. 129, 51–58.
Sierra, A., Gröhn, O., Pitkänen, A., 2015. Imaging microstructural damage and plasticity in the hippocampus during epileptogenesis. Neuroscience 309, 162–172.
Staba, R.J., Frighetto, L., Behnke, E.J., Mathern, G.W., Fields, T., Bragin, A., et al., 2007. Increased fast ripple to ripple ratios correlate with reduced hippocampal volumes and neuron loss in temporal lobe epilepsy patients. Epilepsia 48, 2130–2138.
Steinhauser, C.M., Grunnet, M., Carmignoto, G., 2016. Crucial role of astrocytes in temporal lobe epilepsy. Neuroscience 323, 157–169.
Theyel, B.B., Llano, D.A., Sherman, S.M., 2010. The corticothalamocortical circuit drives higher order cortex in the mouse. Nat. Neurosci. 13, 84–88.
Thom, M., 2014. Hippocampal sclerosis in epilepsy: a neuropathology review. Neuropathology and Applied Neurobiology 40, 520–543.
Tohmi, M., Takahashi, K., Kubota, Y., Hishida, R., Shibuki, K., 2009. Transcranial flavoprotein fluorescence imaging of mouse cortical activity and plasticity. J. Neurochem. 109, 3–9.